Supporting Information

Synergistic nickel phthalocyanine integration on carbon nitride for improved selective nitrogen reduction to ammonia

Sourav Bhowmick,[a,c†] Narad Barman,[b†] Amal Gain,[a†] Ashadul Adalder,[f] Rajashri Urkude,[d] Biplab Ghosh,[d] Sourav Mukherjee[e], Supriya Mondal,[*c] Ranjit Thapa,[*b] Uttam Kumar Ghorai[*a]

[a]Department of Industrial Chemistry & Applied Chemistry, Swami Vivekananda Research Centre, Ramakrishna Mission Vidyamandira, Belur Math, Howrah - 711202, India
*E-mail: uttam.indchem@vidyamandira.ac.in

[b]Department of Physics and Centre for Computational & Integrative Sciences, SRM University AP, Amaravati 522 240 Andhra Pradesh, India
*Email: ranjit.phy@gmail.com

[c]Department of Physics, Government General Degree College Chapra, Nadia, West Bengal, 741123, India
*Email: supriyajuphy@gmail.com

[d]Beamline Development & Application Section, Bhabha Atomic Research Centre, Trombay, Mumbai 400 085, India

[e]School of Physical Sciences, Indian Association for the Cultivation of Science, Jadavpur, Kolkata 700032, India

[f]Department of Chemical Sciences, Indian Institute of Science Education and Research (IISER) Kolkata, Nadia 741246, West Bengal, India

†Equal Contribution

SI 1: Catalyst ink preparation

1.1 mg of each catalyst is dispersed in 100 µL isopropanol solution, and 10 µL Nafion 117 (5% solution) was added to the slurry as a binder and made homogeneous. 1 µL of slurry was dropped on the glassy carbon electrode (loading 0.01 mg on the glassy carbon electrode with a surface area of 0.071 cm^2).

SI 2: Quantitative determination of concentration of ammonium ion

To account for the concentration of ammonia quantitatively, the Indophenol blue method was applied with the help of UV-visible spectroscopy. 2 ml of a solution of 5% salicylic acid, 5% sodium citrate dihydrate (Merck Co., Ltd.), in 1M NaOH solution, 1 ml of 0.05M sodium hypochlorite (Merck Co., Ltd.) solution, and 0.2 ml of a 3.34 mM solution of sodium nitroprusside dihydrate (Loba Chemie Co., Ltd.) were mixed with 2 ml of a solution taken from the electrochemical cell, completing NRR. Incubation was done for the solution for 2 hours at room temperature, and then absorbance was measured. Having maximum absorbance at 655 nm in UV-visible spectroscopy, the formation of indophenol blue can be justified.

The plotting of the calibration batch was done with the variation of ammonium chloride (Merck Co., Ltd.) concentration as 1, 0.8, 0.6, 0.4, 0.2, and 0.0 µg/ml mixed in acidic solution and performed in UV-visible spectroscopy, and a linear relation was observed in the absorbance vs. concentration plot following the equation $y = 0.13614x + 0.0591$, and where $R^2 = 0.999$ (**Fig. S1 (a-b)**).

SI 3: Quantitative estimation of NO_x contaminants

Using *N*–(–1–naphthyl)–ethylenediamine dihydrochloride NO_x was estimated quantitatively in UV-visible spectroscopy. A colorant liquid was composed by mixing of 0.5 g of sulfanilic acid and 5 ml of acetic acid (Merck Co., Ltd.) in Millipore water afterwards addition of 5 mg of *N*–(1–naphthyl)–ethylenediamine dihydrochloride (Loba Chemie Pvt. Ltd.), adjusting the final volume to 100 ml. Then, 1 ml of electrolyte collected during electrochemical process and 4 ml of colorant solution were added, followed by incubation for 15 min and studied in UV-visible spectra analysis. The calibration curves are displayed in **Fig. S1 (c-d)**, received applying sodium nitrite (Merck Co., Ltd.) varying concentration like 1, 0.8, 0.6, 0.4, 0.2 and 0.0 (µg/ml) in 0.1 M H_2SO_4.

SI 4: Quantitative estimation of hydrazine concentration

To estimate hydrazine quantity the Watt and Chrisp method were applied. By using 300 ml of absolute alcohol (Merk Co. Ltd), 30 ml conc. HCl (Merk Co. Ltd) and 5.99g of para(dimethlyamaino)benzaldehyde (Merk Co. Ltd) the colorant solution was prepared which was needed to comply the method. After that, 5ml of this colorant solution and 1ml of specimen solution were taken together followed by 15 min of incubation and with 455nm of maximum absorbance, the UV-visible spectroscopy was performed for that solution.

solution batch for the calibration were prepared in following way: varying the concentration of hydrazine-monohydrate the batch was prepared as standard like 0.0, 0.2, 0.4, 0.6, 0.8 and 1.0 µg/ml (**Fig. S1 (e-f)**). Then 1 ml of prepared standard hydrazine monohydrate and 5ml colorant solution were mixed and agitated for few minutes at room temperature and allowed in dark for further 15 min for incubation. After that it was experimented in UV-visible spectroscopy and absorbance was noted at 455 nm as maximum. The absorbance vs concentration graph showed a linear phenomenon ($y = 0.27643x + 0.02695$; $R^2 = 0.999$) for the absorbance and concentration of hydrazine monohydrate.

SI 5: Determination of Ammonium ion by ion Chromatography

Eco IC Metrohm was used to do ion chromatography. The cationic column Metrosep C 6–150/4.0, used in IC, has a flow rate of 0.9 mL/min. The eluent was a nitric acid solution at 1.7 mmol/L. At a pressure of 7.55 MPa, the ammonium ion retention time was around 5.9 minutes. (**Fig. S9**)

With ammonium sulphate concentrations ranging from 0.0 µg mL^{-1} to 2.0 µg mL^{-1}, the standard calibration curve for ammonium ion detection was employed. The calibration curve's $y = 0.1274x + 0.0049$ equation was used to determine the ammonium ion concentration (**Fig. S9 b**).

SI 6: Computational details

All the required theoretical findings are performed using VASP, a computational code, based on density functional theory (DFT). To expand all the electronic waves, a plane wave basis set[1] is incorporated within a maximum kinetic energy cut-off of 450 eV. The energy and force convergence criteria, for optimizing all the structures, were set to be 10^{-05} eV and 10^{-04} eV/Å respectively. The interactions between frozen core and outer electrons were treated through projector augmented wave method. The exchange and correlation effects of electrons were

approximated by generalized gradient approximation (GGA) in Perdew-Burke-Ernzerhof (PBE)[2] form. As long-range weak Van der Waal forces among atoms in the system cannot be ruled out, Grimme DFT-D2 dispersion[3] scheme has been considered. Brillouin zones were sampled by Gamma centre k-point mess in case of structural optimization and electronic calculations (PDOS).

The free energy calculations, ΔG after the adsorption of nitrogen containing intermediates (N_2, N_2H, or N_xH_y) are obtained using the following equations[4]:

$$\Delta G = \Delta E_{NxHy} + \Delta ZPE - T\Delta S + \Delta G_U + \Delta G_{pH} \quad \ldots\ldots\ldots\ldots (1)$$

$$\Delta G_U = -eU \quad \ldots\ldots\ldots\ldots\ldots (2)$$

$$\Delta GpH = ln10k_BT \times pH \quad \ldots\ldots\ldots\ldots\ldots (3)$$

where ΔE, ΔZPE, S, T, e, k_B and U are the adsorption energy, change of the zero-point energy (ZPE), entropy, temperature, elementary charge constant, Boltzmann's constant, and electrode potential, respectively. In this work, we consider $T = 300\ K$ and acidic environment i.e. $pH = 0$. The adsorption energy ΔE_{NxHy} is given as:

$$\Delta E_{NxHy} = E_{*NxHy} - E^* - E_{Nx} - \left(\frac{y}{2}\right) \times E_{H2} \quad \ldots\ldots\ldots\ldots\ldots (4)$$

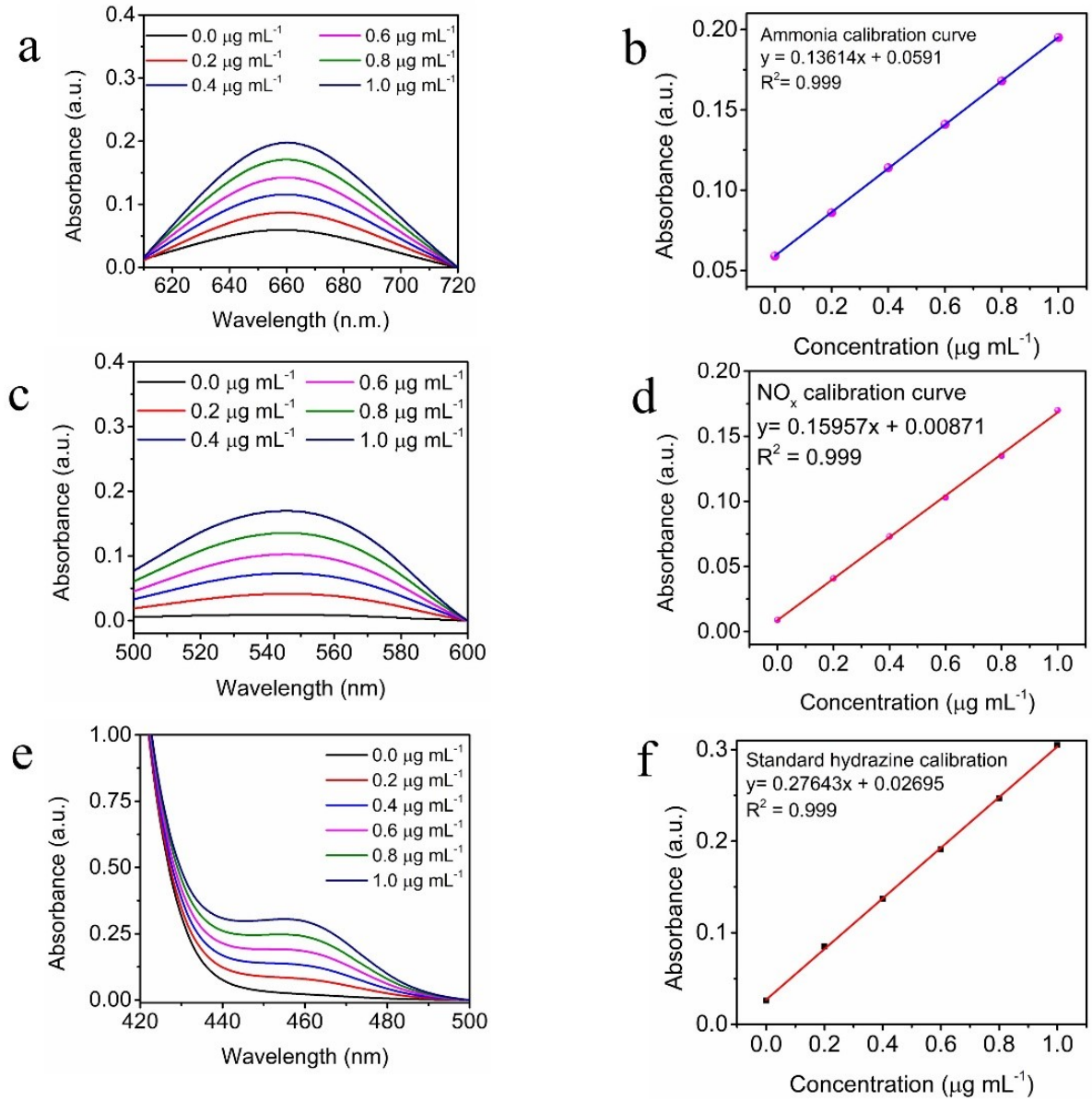

Fig. S1: (a-b) Standard calibration of ammonia solution, (c-d) Standard calibration of NO_x, (e-f) Standard calibration of hydrazine

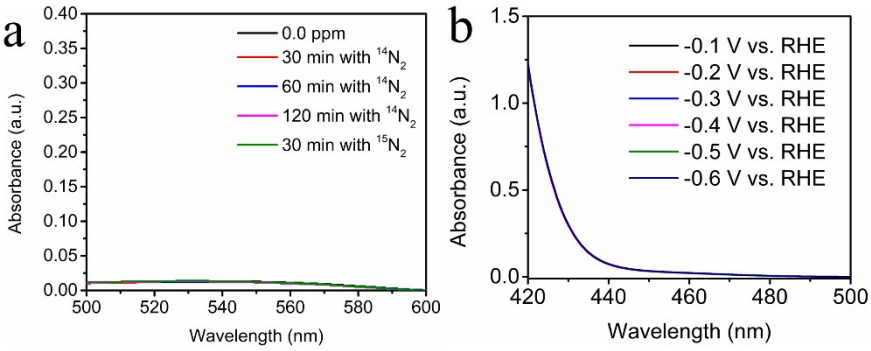

Fig. S2: (a) Detection of the NO_x in the electrolyte, (b) Detection of hydrazine produced during eNRR process.

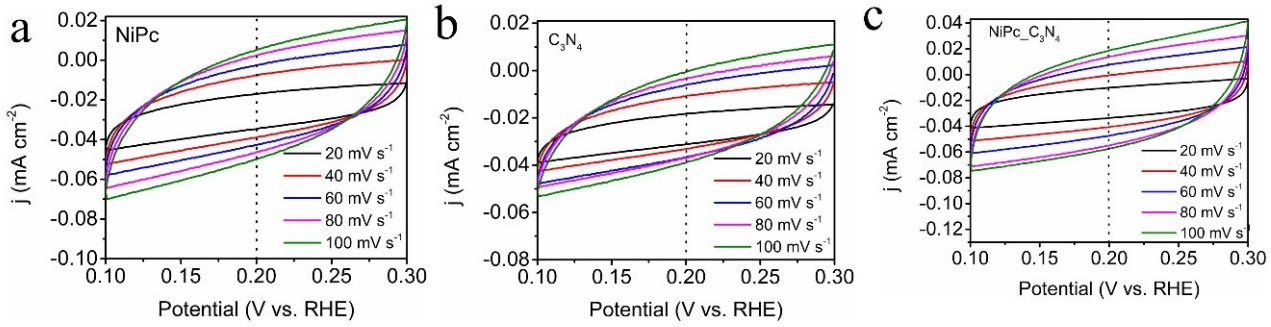

Fig. S3: CV plots of the catalyst: (a) NiPc, (b) C_3N_4, (c) NiPc_C_3N_4

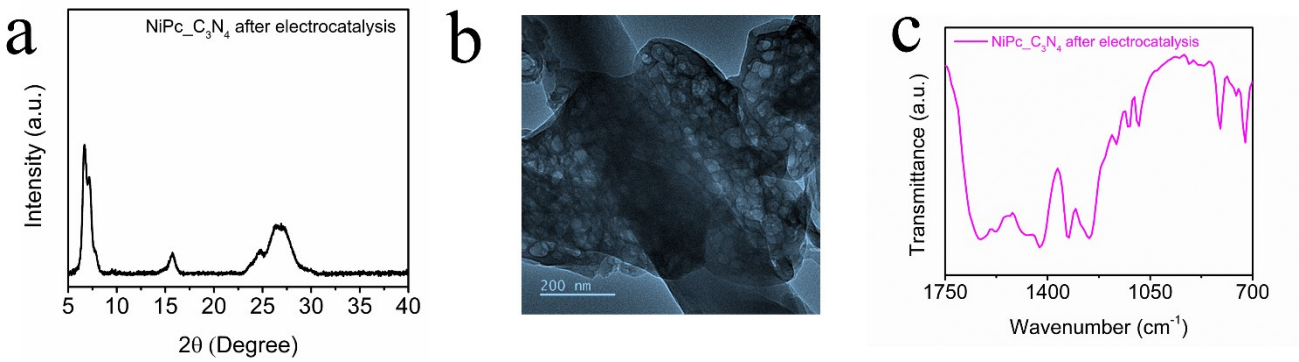

Fig. S4: (a) XRD (b) TEM and (c) FTIR plot of NiPc_C_3N_4 after electrochemical reaction

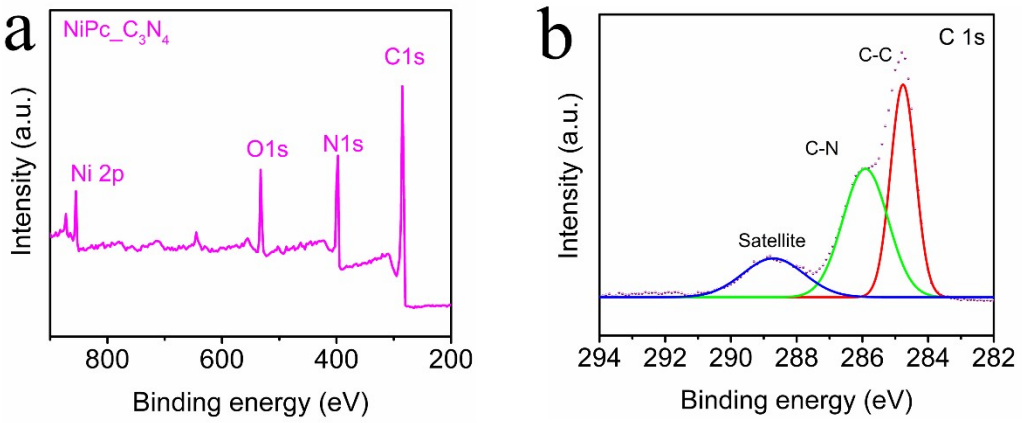

Fig. S5: (a) XPS survey scan of NiPc_C_3N_4 and (b) HR scan of C 1s of NiPc_C_3N_4

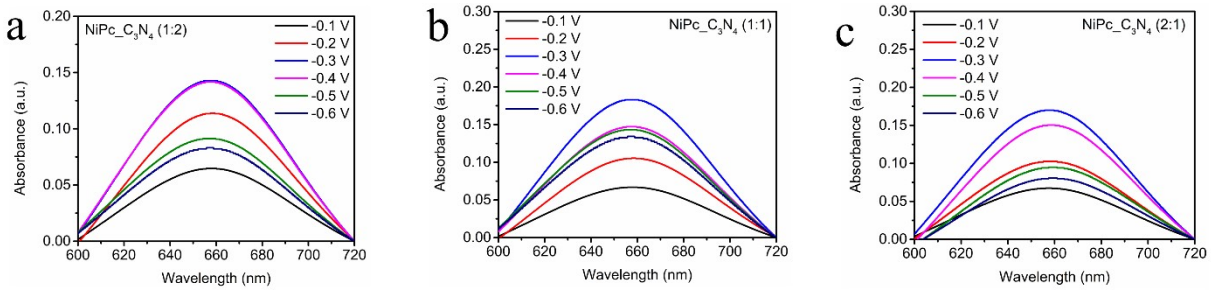

Fig. S6: UV-Vis curve of produced ammonia by Indo-phenol blue method of (a) NiPc_C_3N_4(1:2) (b) NiPc_C_3N_4(1:1) (c) NiPc_C_3N_4(2:1)

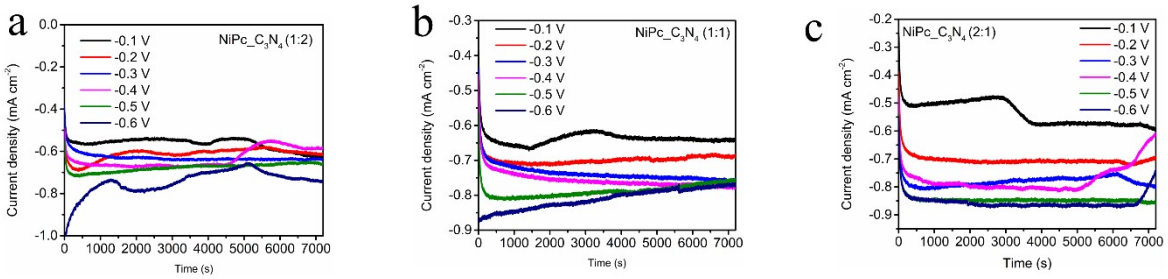

Fig. S7: Chronoamperometric j vs t curve of (a) NiPc_C_3N_4(1:2) (b) NiPc_C_3N_4(1:1) (c) NiPc_C_3N_4 (2:1).

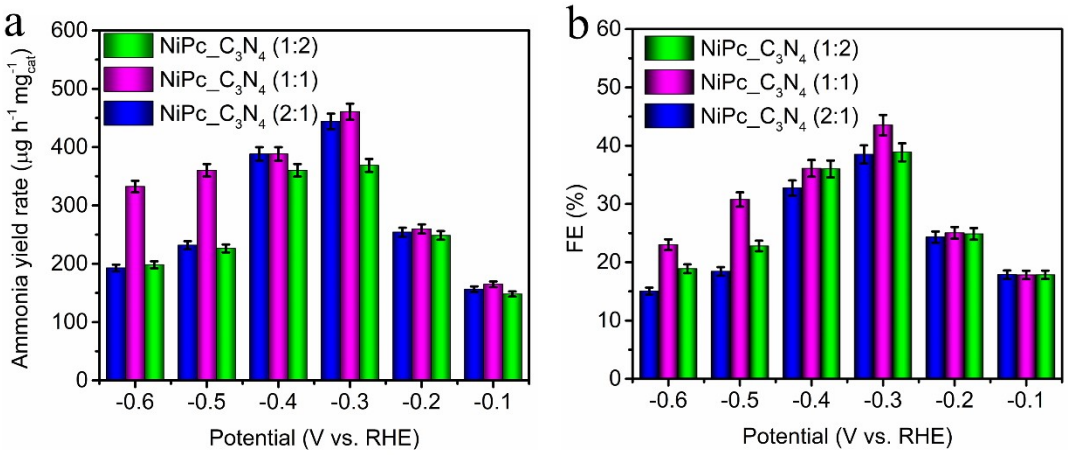

Fig. S8: (a) Yield rate and (b) FE of produced ammonia during eNRR by NiPc_C_3N_4(1:2), NiPc_C_3N_4 (1:1) and NiPc_C_3N_4 (2:1) respectively.

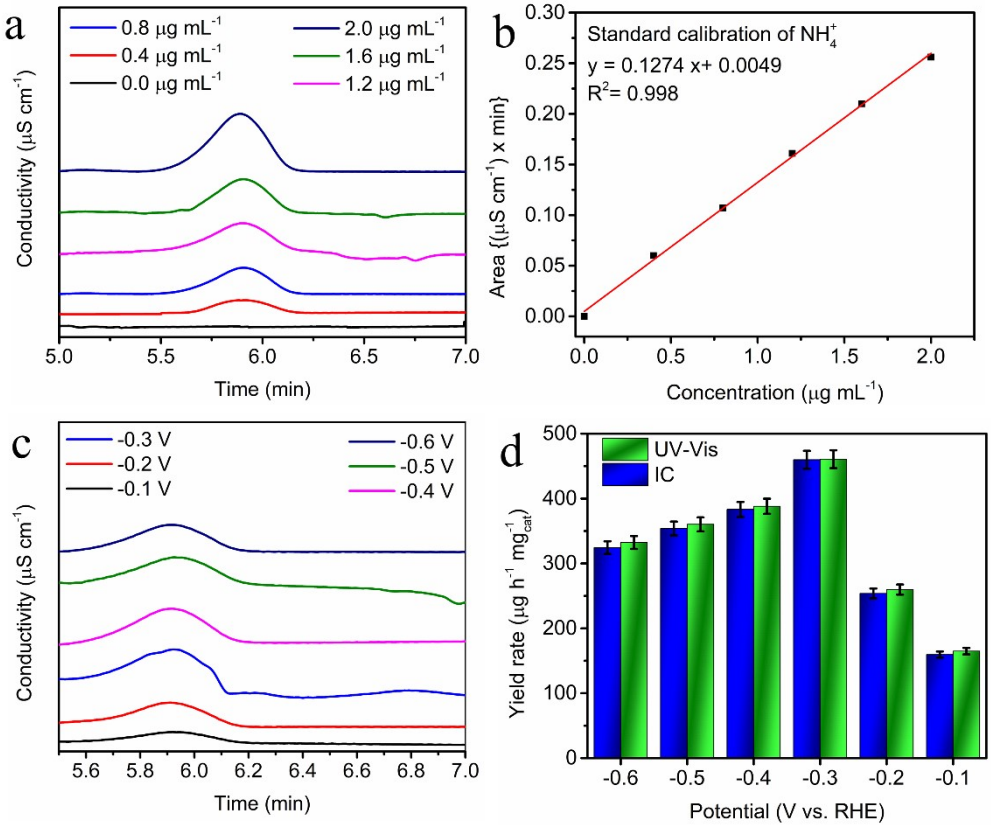

Fig. S9: (a) Conductivity vs time plot of various standard samples of ammonium ion from ion chromatography (b) Calibration curve of ammonia from standard ammonia sample (c) Conductivity vs time plot of electrolyte after eNRR reaction of NiPc_C_3N_4 (d) Comparison of yield rate of ammonia determined by UV-Vis method and IC method of NiPc_C_3N_4.

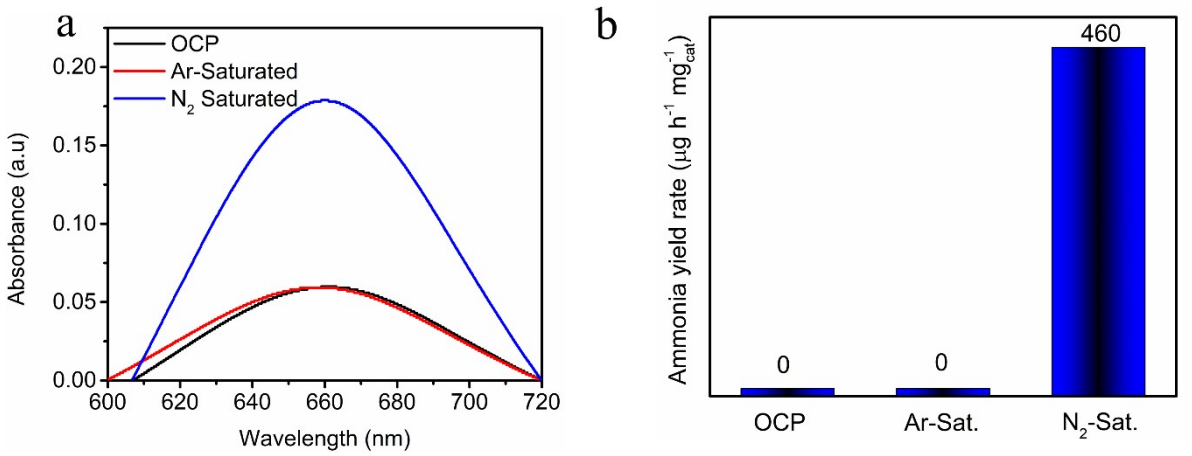

Fig. S10: Control experiments: (a) UV-Vis curve (b) yield rate of ammonia in Ar saturated, N_2 saturated and open circuit (OCP) condition using NiPc_C_3N_4 catalyst.

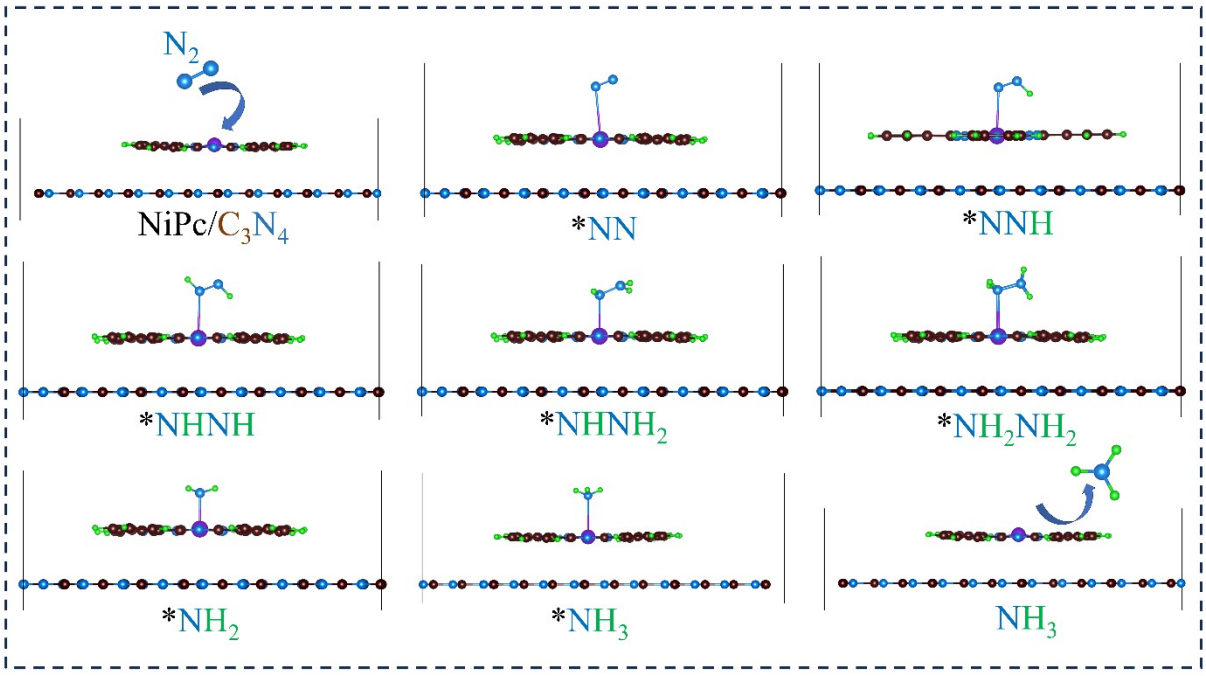

Fig. S11: Optimized intermediate states during e-NRR on NiPc/C_3N_4.

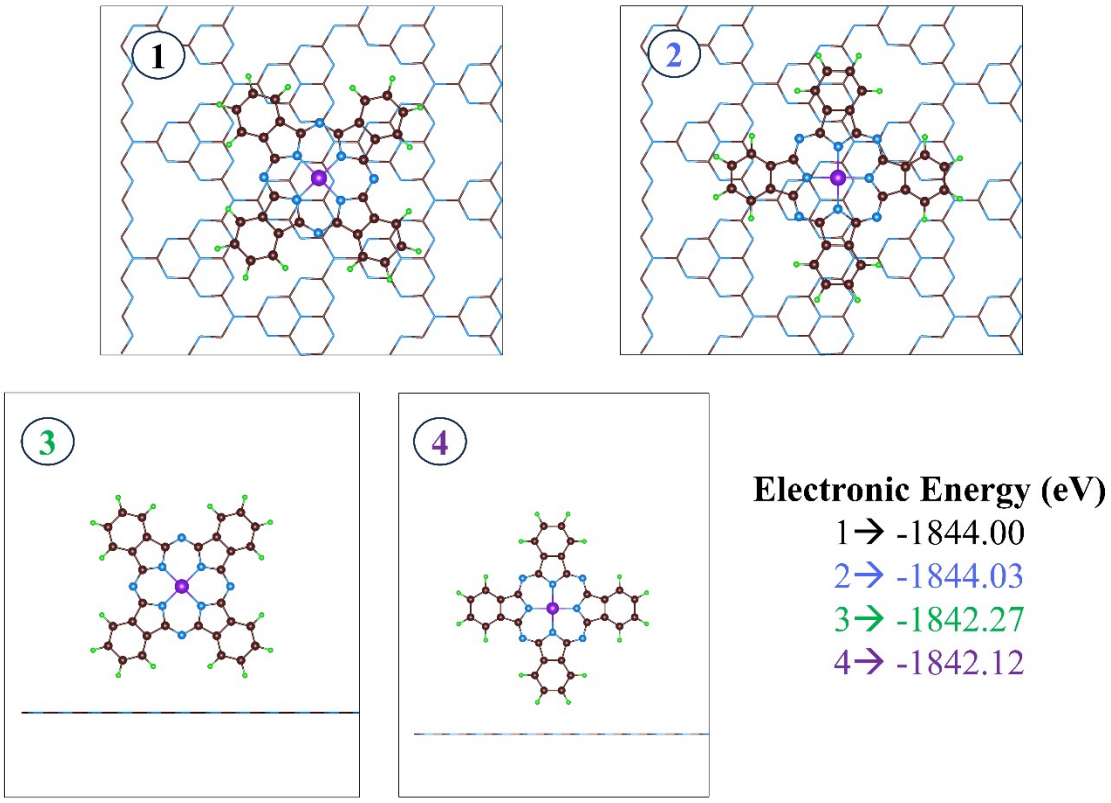

Fig. S12: (1), (2), (3) and (4) are optimized structures of $NiPc/C_3N_4$ with four possible configurations.

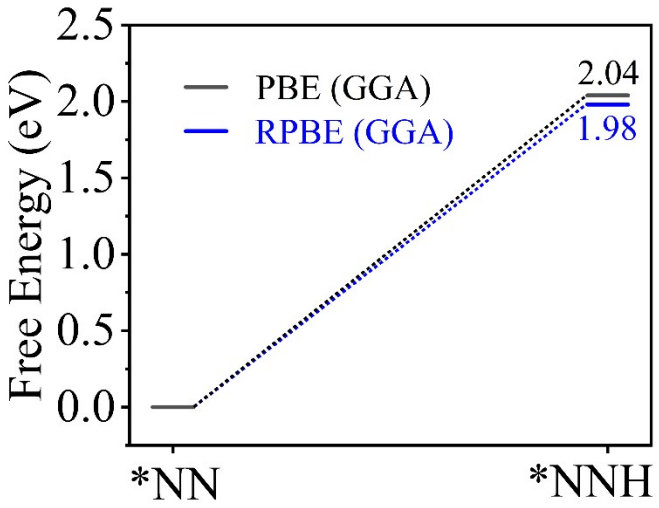

Fig. S13: Investigation of limiting potential with two different functionals (PBE and RPBE).

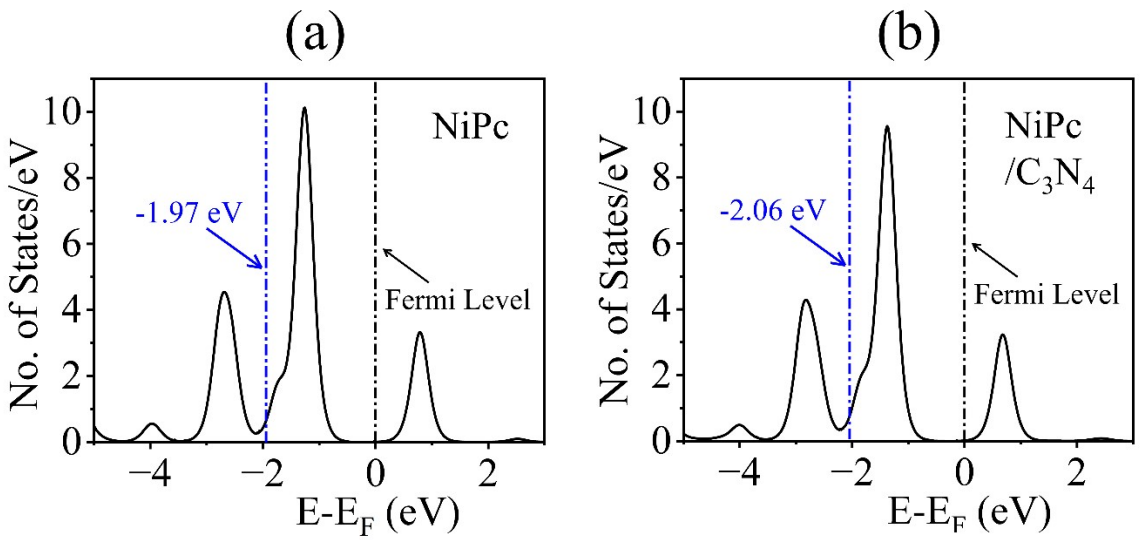

Fig. S14: (a) and (b) represent the d-band centre of Ni in NiPc and NiPc/C_3N_4 respectively.

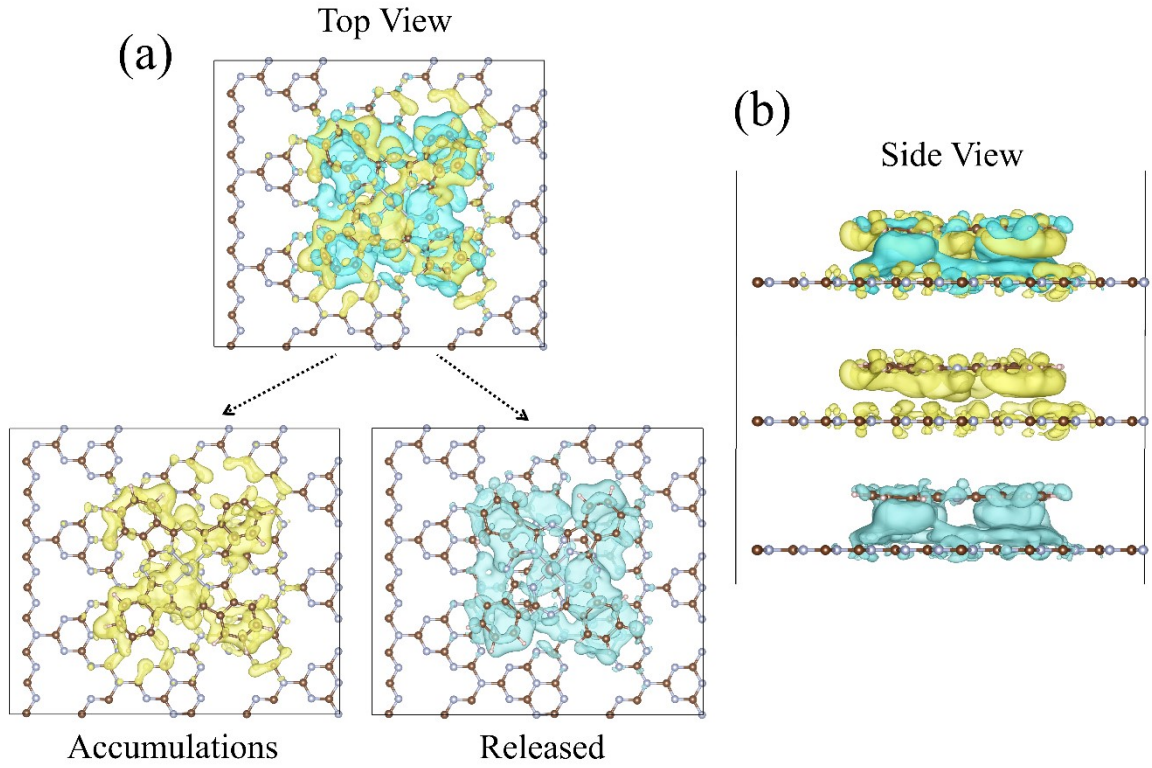

Fig. S15: (a) and (b) represent top and side view of charge density difference after addition of 2d layer of C_3N_4 with NiPc respectively.

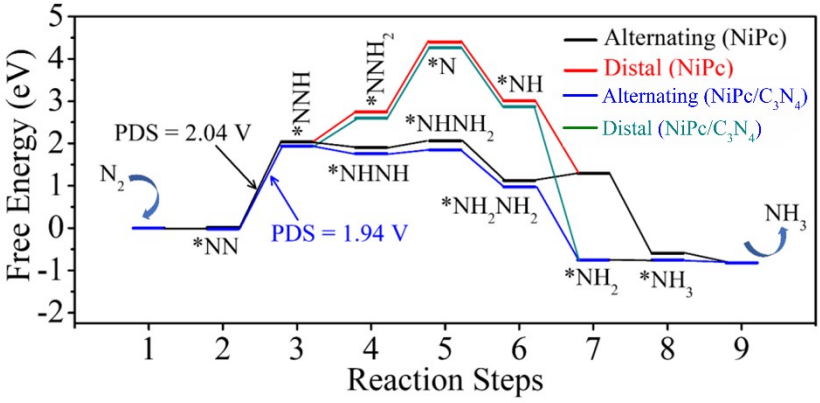

Fig. S16: Free Energy vs. Reaction steps diagram

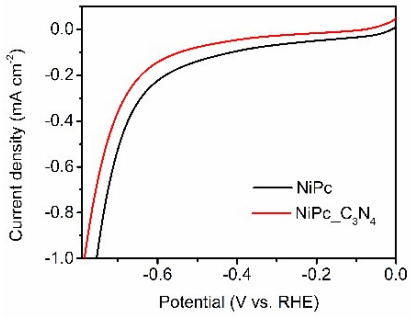

Fig. S17: LSV plot of NiPc and NiPc_C_3N_4 in Argon saturated atmosphere.

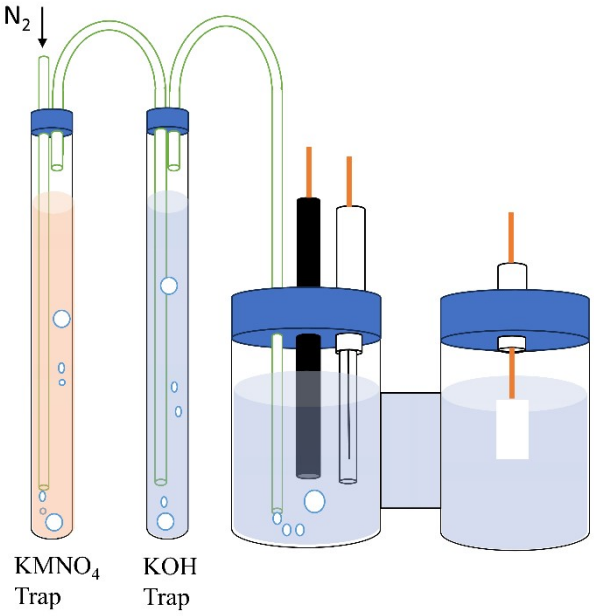

Fig. R18: Schematic representation of gas purification system prior electrochemical reaction

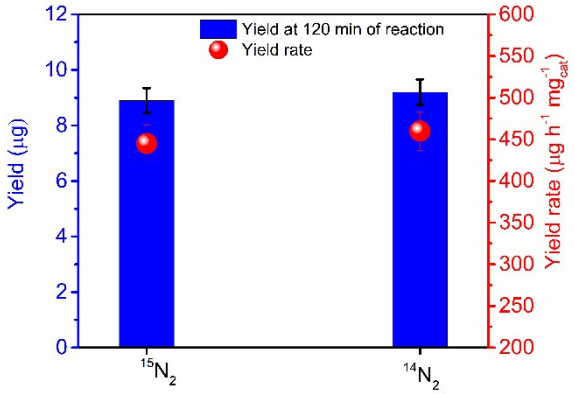

Fig. S19: yield comparison between $^{15}N_2$ and $^{14}N_2$ source

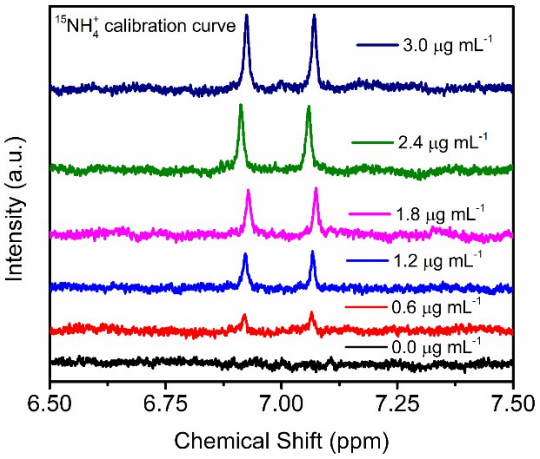

Fig. S20: $^{15}NH_4^+$ calibration series through ^{1}H-NMR

Table-S1

Adsorbed Molecules	ZPE-TS (eV)
NN	0.05
NNH	0.08
NHNH	0.47
$NHNH_2$	0.79
NH_2NH_2	1.12
NH_2	0.49
NH_3	0.69
NNH_2	0.49
N	-0.05
NH	0.14

Table S2: ammonia yield at different condition

Condition	NH_3 yield (μg)
$^{14}N_2$ purged static electrolyte without reaction (purged time 120 min)	0.04
30 min of reaction with $^{14}N_2$	2.19
60 min of reaction with $^{14}N_2$	4.40
120 min of reaction with $^{14}N_2$	9.02

Table S3: NO_x concentration at different condition

Condition	NO_x concentration
30 min of $^{14}N_2$ purging without reaction	Same as background intensity
60 min of $^{14}N_2$ purging without reaction	Same as background intensity
120 min of $^{14}N_2$ purging without reaction	Same as background intensity
30 min of $^{15}N_2$ purging without reaction	Same as background intensity

Table S4: Comparison of the NRR activity of various transition metal based electro-catalyst in solution media of varying pH under ambient conditions

Catalyst	Electrolyte	Potential (V vs RHE)	NH_3 yield	FE (%)	References
MoS_2	0.1 M Na_2SO_4	− 0.5 V	8.08×10^{-11} mol s^{-1} cm^{-2}	1.17 %	*Adv. Mater.* **2018**, *30*, 1800191
MoS_2 nanoflowers	0.1 M Na_2SO_4	− 0.40 V	29.28 μg h^{-1} mg^{-1}_{cat}	8.34 %	*Adv. Energy Mater.* **2018**, *8*, 1801357
Mo_2C/C	0.5 M Li_2SO_4	− 0.3 V	11.3 μg h^{-1} mg^{-1}_{cat}	7.8 %	*Adv. Mater*. **2018**, *30*, 1803694
a-Au/CeO_x–RGO	1 M HCl	− 0.2 V	8.3 μg h^{-1} mg^{-1}_{cat}	10.1 %	*Adv. Mater*. **2017**, *29*, 1700001
Au nanorods	0.1 M KOH	− 0.2 V	1.648 μg h^{-1} cm^{-2}	4.02 %	*Adv. Mater*. **2017**, *29*, 1604799
$Pd_{0.2}Cu_{0.8}$/RGO	0.1 M KOH	− 0.2 V	2.80 μg h^{-1} mg^{-1}_{cat}	~4.3 %	*Adv. Energy Mater*. **2018**, *8*, 1800124
Au-TiO_2	0.1 M HCl	− 0.2 V	21.4 μg h^{-1} mg^{-1}_{cat}	8.11 %	*Adv. Mater*. **2017**, *29*, 1606550
W_2N_3 nanosheet	0.10 M KOH	− 0.2 V	11.66 ±0.98 μg h^{-1} mg^{-1}_{cat}	11.67 ± 0.93 %	*Adv. Mater*. **2019**, *31*, 1902709
NiO/G	0.1 M Na_2SO_4	− 0.7 V	18.6 μg h^{-1} mg^{-1}_{cat}	7.8 %	*ACS Appl. Energy Mater.* ***2019***, *2, 3, 2288–2295*
Nb_2O_5 nanofiber	0.1 M HCl	− 0.55 V	43.6 μg h^{-1} mg^{-1}_{cat}	9.26 %	*Nano Energy*, **2018**, *52*, 264-270

Mo doped MnO_2 nanoflowers	0.1 M Na_2SO_4	− 0.5 V	36.6 μg h^{-1} mg^{-1}_{cat}	12.1% (-0.4 V)	*Appl. Catal. B*, **2020**, *264*, 118525
Cr_2O_3 microspheres	0.1 M Na_2SO_4	– 0.9 V	25.3 μg h^{-1} mg^{-1}_{cat}	6.78 %	*ACS Catal*. **2018**, *8, 9*, 8540-8544
FePc/C	0.1 M Na_2SO_4	− 0.3 V	10.25 μg h^{-1} mg^{-1}_{cat}	10.50%	*ACS Catal. **2019**, 9, 8, 7311–7317*
Fe-CeO_2	0.5 M $LiClO_4$	− 0.5 V	26.2 μg h^{-1} mg^{-1}_{cat}	14.7% (−0.4 V)	*J. Mater. Chem. A*, **2020**, *8*, 5865-5873
CoO-QD/RGO	0.1 M Na_2SO_4	− 0.6 V	21.5 μg h^{-1} mg^{-1}_{cat}	8.3 %	*J. Mater. Chem. A*, **2019**, *7*, 4389-4394
TiO_2-RGO	0.1 M Na_2SO_4	– 0.90 V	15.13 μg h^{-1} mg^{-1}_{cat}	3.3 %	*J. Mater. Chem. A*, **2018**, *6*, 17303-17306
FePc/O-MWCNT	0.1 M HCl	− 0.3 V	36 μg h^{-1} mg^{-1}_{cat}	9.73 %	*Chem. Commun*. **2019**, *55*, 14111
Mn_3O_4 nanocubes	0.1 M Na_2SO_4	− 0.8 V	11.6 μg h^{-1} mg^{-1}cat	3.0 %	*Small,* **2018**, *14*, 1803111
Spinel $LiMn_2O_4$ nanofiber	0.1 M HCl	− 0.50 V	15.83 μg h^{-1} mg^{-1}_{cat}	7.44%	*Inorg. Chem. **2019**, 58, 15, 9597–9601*
Zr^{4+}-doped TiO_2	0.1M KOH	− 0.45 V	8.90 μg h^{-1} cm^{-2}	17.3%	*Nat. Commun*. **2019**, *10*, 2877
NCM-Au NPs	0.1 M HCl	-0.2 V	0.36 g m^{-2} h^{-1}	22%	*Angew. Chem. Int. Ed*. **2018**, *57*, 12360–12364
CoPc NTs	0.1 M HCl	− 0.3 V	107.9 μg h^{-1} mg^{-1}_{cat}	27.7%	*ACS Nano.* **2021,** 15, 3, 5230–5239
Mo-Co/NC	0.1 M Na_2SO_4	–0.1V	89.8 μmol h^{-1} g_{cat}^{-1}	13.5%	*J. Mater. Chem. A,* **2020**, 8, 9091.
(Ni_x-N-C)	0.5 M $LiClO_4$	–0.8 V	115 μg cm^{-2} h^{-1}	-	*Small Methods, **2020**, 4, 1900821*
(N-NiO/CC)	0.1 M $LiClO_4$	−0.5 V	22.7 μg h^{-1} mg^{-1}	7.3%	*ChemCatChem,* **2019**, 11, 4529
(NiO/G)	0.1 M Na2SO4	−0.7 V	18.6 μg h^{-1} mg^{-1}	7.8%	*ACS Appl. Energy Mater*. **2019**, 2, 2288.

NiPc	0.1 M HCl	–0.3V	85 μg $h^{-1}mg^{-1}_{cat}$	25%	*J. Mater. Chem. A,* **2021**, 9, 14477
NiPc_C_3N_4	**0.05 M H_2SO_4**	**–0.3V**	**460 ± 14 μg $h^{-1}mg^{-1}_{cat}$**	**43 ± 1 %**	***This Work***

References:

1 G. Kresse and J. Furthmiiller B ', *Efficiency of ab-initio total energy calculations for metals and semiconductors using a plane-wave basis set*, 1996, vol. 6.

2 J. P. Perdew, K. Burke and M. Ernzerhof, *Generalized Gradient Approximation Made Simple*, 1996.

3 S. Grimme, *J Comput Chem*, 2006, **27**, 1787–1799.

4 J. K. Nørskov, T. Bligaard, A. Logadottir, J. R. Kitchin, J. G. Chen, S. Pandelov and U. Stimming, *J Electrochem Soc*, 2005, **152**, J23.